ACS Chemical Neuroscience

pubs.acs.org/chemneuro Research Article

A Single Silicon Nanowire-Based Ratiometric Biosensor for Ca^{2+} at Various Locations in a Neuron

Min Chen, Lixuan Mu,* Shuai Wang, Xingxing Cao, Sen Liang, Yuan Wang, Guangwei She, Jun Yang, Yongan Wang, and Wensheng Shi

Cite This: *ACS Chem. Neurosci.* 2020, 11, 1283−1290 Read Online

ACCESS | Metrics & More | Article Recommendations | Supporting Information

ABSTRACT: Ionic calcium (Ca^{2+}) is an important second messenger in cells, particularly in the neuron. A deficiency or excess of Ca^{2+} would lead to neuronal apoptosis and further injury to the brain. For accurate analysis of intracellular Ca^{2+}, a single silicon nanowire (SiNW)-based ratiometric biosensor was constructed by simultaneously anchoring $Ru(bpy)_2$(mcbpy-O-Su-ester)$(PF_6)_2$, as a reference molecule, and Fluo-3, as a response molecule, onto the surface of a single SiNW. The SiNW-based biosensor exhibits high sensitivity and favorable selectivity for detecting Ca^{2+}. With the assistance of a micromanipulator and laser scanning confocal microscope, two single SiNW sensors were placed in the body and the neurites of an individual neuron to detect Ca^{2+}. The difference between the concentrations of Ca^{2+} in the body and neurites was identified. The results from the present study provide new insights into Ca^{2+} in neurons at a high spatial resolution, and the strategy used in this study provides a new opportunity to investigate cellular metabolism by combining the advantages of a single-cell detection technique and physiology.

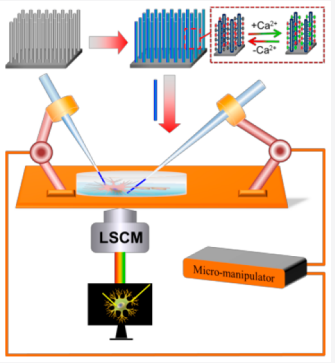

KEYWORDS: *Calcium detection, silicon nanowires, ratiometric fluorescent sensors, micromanipulation, individual neuron*

INTRODUCTION

As an important second messenger in cells, intracellular Ca^{2+} signaling is related to many cellular activities, for example, managing the activation of ion channels in the plasma membrane and cell death.[1−3] In particular, intracellular Ca^{2+} regulates fundamental processes in neurons, such as plasticity and synaptic transmission.[4−6] Upon exposure to various stimuli, the cellular Ca^{2+} concentration increases from the low level that is characteristic of the resting state to a higher level.[7] The dysregulation of Ca^{2+} homeostasis can lead to neurodegenerative diseases, skeletal muscle defects, and chronic heart failure.[8] Ca^{2+} is not distributed uniformly throughout the cell, and only a few Ca^{2+} ions in the cytoplasm are freely diffusible.[9] Therefore, the ability to detect Ca^{2+} in a single cell with high spatial resolution is a prerequisite for the investigation of the fluctuation of Ca^{2+} and to obtain insights into the Ca^{2+}-related processes in neurons, particularly in the body and neurites of a single neuron.

Fluorescence sensors are usually used to measure intracellular Ca^{2+}, including genetically encoded calcium indicators,[10] small-molecule fluorescence probes,[11−13] and nanoparticles.[14,15] The genetically encoded fluorescent indicators usually involve complex transfection steps.[16] Moreover, the leakage of small-molecule fluorescent probes from the cell and the drift of the nanoparticles in cells, as well as the inhomogeneous distribution of the molecules and nanoparticles in a cell,[17−19] also prevent researchers from accurately profiling the heterogeneity of Ca^{2+} in an individual cell at a high spatial resolution.[20−22] Therefore, a sensor with new configuration must be developed for the accurate and stable detection of the Ca^{2+} in a single cell.

A one-dimensional (1D) nanostructure is nanometers in diameter and micrometers in length and could be physically located within a single cell.[1,23−26] Accordingly, 1D nanostructures could be used as substrates to anchor small molecule probes to configure a 1D fluorescence sensor.[27,28] By being physically locating in a single cell, the 1D fluorescence sensor could avoid the leakage of small molecules and drift of nanoparticles. Among the various 1D nanostructures, silicon nanowires (SiNWs) exhibit favorable biocompatibility, modifiability, and compatibility with Si technology.[25,26,29,30] SiNW-based sensors have been cleverly used to detect hypochlorous acid in single macrophages.[31] In the present study, SiNWs were chosen as carriers to construct a ratiometric sensor for evaluating intracellular Ca^{2+} with high spatial resolution. The ruthenium-based dye bis(2,2′-bipyridine)-4′-methyl-4-carboxybipyridine-ruthenium *N*-succinimidyl ester-bis-(hexafluorophosphate) ($Ru(bpy)_2$(mcbpy-O-Su-ester)$(PF_6)_2$) with red emission was employed as the reference molecule

Received: January 21, 2020
Accepted: April 15, 2020
Published: April 15, 2020

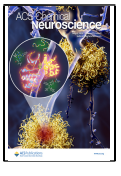

(Ru), and Fluo-3[32] was selected as the response molecule to detect Ca^{2+}.[33] Both the response and reference molecules were covalently immobilized on the surface of the SiNWs, and the SiNW-based Ca^{2+} ratiometric sensor was obtained. The chelation of Ca^{2+} with the response molecule Fluo-3 increases the green emission of the sensor, while the red emission from the reference molecules is not altered. With the assistance of a micromanipulator and laser scanning confocal microscope (LSCM), two single SiNW sensors (SiNW-S) were placed in an individual neuron, and the difference between the concentrations of Ca^{2+} in the cell body and neurite was determined. This new sensor avoids not only the leakage and drift of small molecule or nanoparticle-based fluorescent probes from the cell but also the complex transfection steps in genetically encoded calcium indicators. Especially, this nanowire-based sensor can be positively located in target regions of a cell with the aid of the micromanipulator. The method presented here will provide new insights into Ca^{2+} signal transduction in neurons with a high spatial resolution and low background.

RESULTS AND DISCUSSION

Figure 1a–d shows the SEM images of SiNWs. The lengths of short SiNWs (Figure 1a,b) and long SiNWs (Figure 1c,d) are

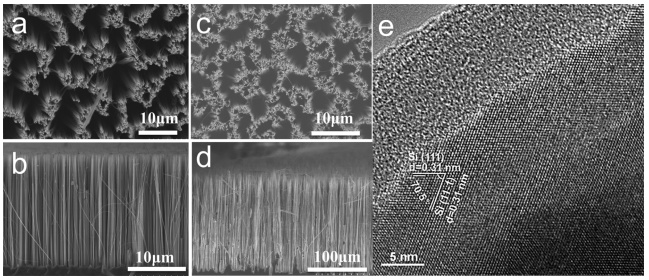

Figure 1. SEM images (a) in top view and (b) in side view of short SiNWs; SEM images (c) in top view and (d) in side view of long SiNWs; (e) HRTEM image of the SiNW.

approximately 20 and 150 μm, respectively. The TEM image (Figure 1e) demonstrates that the SiNW consists of a crystalline Si core and a silica sheath with a thickness of 10 nm.

To fabricate the SiNWs sensor for Ca^{2+}, the obtained SiNWs arrays on a Si wafer (SiNWs-a) were successively hydroxylated (SiNWs-a-OH) and decorated with 3-aminopropyltriethoxysilane (APTES) (SiNWs-a-NH_2), $Ru(bpy)_2$(mcbpy-O-Su-ester)$(PF_6)_2$(SiNWs-a-Ru), and Fluo-3 (SiNWs-A). The procedure for SiNW modification is shown in Scheme 1.

To confirm that the SiNWs-a was decorated with the dyes, we investigated the surface composition of the bare SiNWs-a, SiNWs-a-NH_2, SiNWs-a-Ru, and SiNWs-A by XPS, and the results are shown in Figure S1a. Compared with SiNWs-a, the XPS spectrum of SiNWs-a-NH_2 revealed an obvious peak for nitrogen (Figure S1b), verifying that the surface of the SiNWs was modified with APTES in the first step of Scheme 1. Compared with the XPS spectrum of SiNWs-a-NH_2, the spectrum of SiNWs-a-Ru contained a new fluorine peak (Figure S1c), indicating that $Ru(bpy)_2$(mcbpy-O-Su-ester)-$(PF_6)_2$ was grafted on the surface of SiNWs-a-NH_2 in the second step of SiNWs modification. The peaks of ruthenium and phosphor were not obviously detected, due to a low content of $Ru(bpy)_2$(mcbpy-O-Su-ester)$(PF_6)_2$ modified on the SiNWs. A new chlorine peak was identified in the XPS spectrum of SiNWs-A (Figure S1d), which was attributed to the final decoration of Fluo-3 on the SiNWs. The metal chloride peak in the XPS spectrum of SiNWs-a-Ru was possibly caused by the chelation of chloride in PBS buffer with ruthenium.[34] Based on these observations, both the reference molecule and Fluo-3 were successfully anchored to the surface of the SiNWs.

First, the SiNWs-A was used as a platform for detecting Ca^{2+}. The SiNWs-A (0.5 cm × 0.5 cm) was immersed upside down in phosphate buffer (10 mM, pH = 7.3) in a dish. The fluorescence images of the SiNWs-A were recorded by using a Nikon A1 LSCM with an oil 60× objective lens and laser with an excitation wavelength of 488 nm before and after addition of Ca^{2+}. The fluorescence images of SiNWs-A (Figure 2a1,b1)

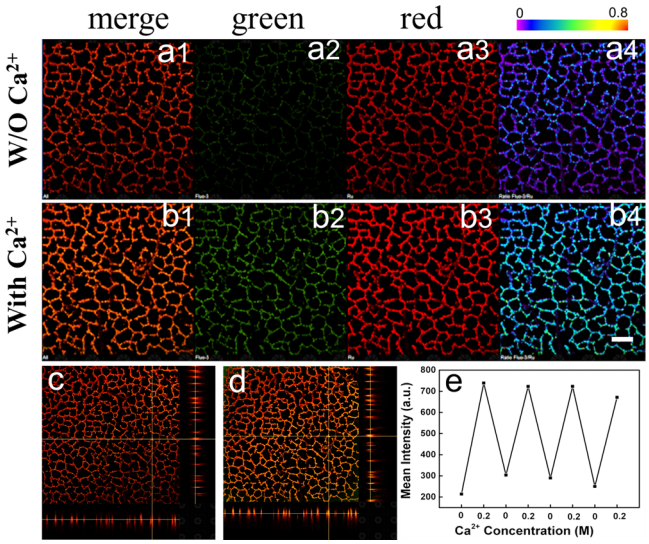

Figure 2. Fluorescence images of SiNWs-A before (a) and after (b) the addition of 500 μM Ca^{2+} in PBS buffer: (a1, b1) fluorescence images in merged channel; (a2, b2) fluorescence images in green channel; (a3, b3) fluorescence images in red channel; (a4, b4) fluorescence ratio images. Slice view of Z-scan fluorescence images of SiNWs-A before (c) and after (d) the addition of 500 μM Ca^{2+}. (e) Reversibility of the green fluorescence of the SiNWs-A at the Ca^{2+} concentrations between 0 to 0.2 M; 10 mM PBS buffer, pH = 7.3, λ_{ex} = 488 nm, RT. The scale bar represents 10 μm.

were separated to different channels: merge channel, green channel, and red channel. As shown in Figure 2a2, weak green fluorescence was observed from the SiNWs-A before the addition of Ca^{2+}. However, the addition of Ca^{2+} significantly increased the green fluorescence of the SiNWs-A (Figure 2b2), and little change in the red fluorescence from the reference molecules was detected (Figure 2a3,b3). The fluorescence ratio images are shown in Figure 2a4,b4. This color change of

Scheme 1. Procedure for SiNWs Modification

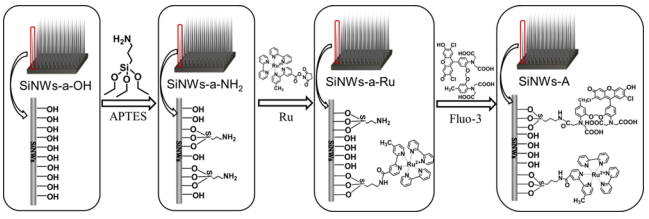

https://dx.doi.org/10.1021/acschemneuro.0c00041
ACS Chem. Neurosci. 2020, 11, 1283–1290

the ratio images demonstrates that the SiNWs-A can be used to detect Ca^{2+}. A series of fluorescence images of Z-scan of the SiNWs-A was also captured before and after the addition of Ca^{2+}. And the slices view of the Z-scan fluorescence images is shown in Figure 2c,d. These fluorescence images further confirm that the two dyes have been successfully modified on the whole array, not just its top. Furthermore, the intensity of the green fluorescence decreased when the SiNWs-A was immersed in the PBS buffer without Ca^{2+} again, indicating that the change in the intensity of the green fluorescence is reversible as the Ca^{2+} concentration changes. Four cycles were executed by altering Ca^{2+} concentrations from 0 to 0.2 M, and the reversibility of the green fluorescent was consistent, as shown in Figure 2e. The distinct response of the SiNWs-A to Ca^{2+} implies that the SiNWs-A could be developed as a device to reversibly monitor the Ca^{2+}.

Next, we investigated the response of the SiNW-S, which was dropped off from the SiNWs-A, to Ca^{2+}. A 10 μL stock solution of the SiNW-S was added to a dish containing 1 mL of PBS buffer (10 mM, pH = 7.3), and the system was stabilized for 10 min. Then, fluorescence images of the SiNW-S were captured by using a Nikon A1 LSCM. As shown in Figure 3a–c, only red fluorescence was observed from the SiNW-S before the addition of Ca^{2+}. However, the SiNW-S exhibited orange fluorescence emission after Ca^{2+} was added to the solution (Figure 3d). By observing the fluorescence from the green and red channels and comparing them with fluorescence of the SiNW-S without Ca^{2+}, we found that the green emission was increased by the Ca^{2+} (Figure 3b,e), and the red fluorescence exhibited little change (Figure 3c,f), causing the emergence of the orange fluorescence emission. And the appearance of fluorescence change of SiNW-S demonstrates that the SiNW-S also has distinct response to Ca^{2+} in PBS solutions.

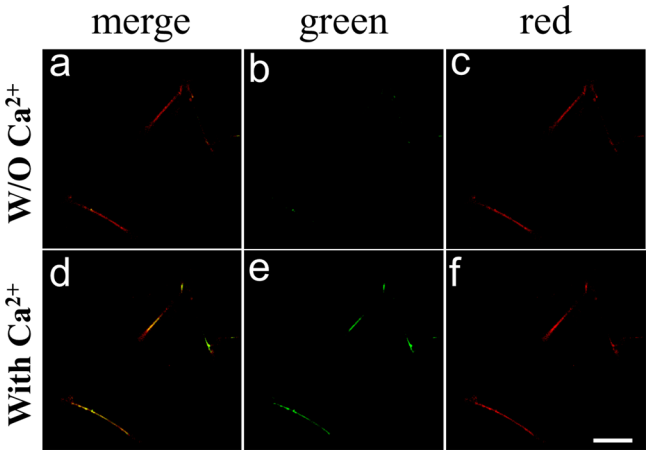

Figure 3. Fluorescence images of the SiNW-S. (a–c) SiNW-S in PBS without Ca^{2+}; (d–f) SiNW-S in PBS supplemented with Ca^{2+}; (a, d) images from merge channel; (b, e) images from green channel; (c, f) images from red channel. The red and green lines represent the fluorescence of SiNW-S in red and green channels, respectively. Conditions: 10 mM PBS solution, pH = 7.3; laser with an excitation wavelength of 488 nm, RT. The scale bar represents 10 μm.

We investigated the selectivity and anti-interference ability of the SiNW-S. As shown in Figure 4, the addition of Mg^{2+}, Zn^{2+}, K^+, and Na^+ ions to the SiNW-Ss solution had little effect on the normalized ratio of green and red fluorescence intensities (I_{green}/I_{red}) of the SiNW-Ss (black bar). Thus, the

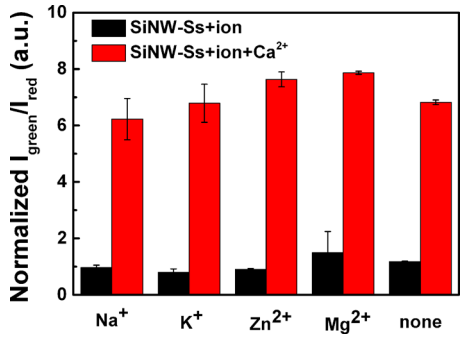

Figure 4. Normalized ratio of fluorescence intensity of the SiNW-Ss incubated with 0.1 mM Na^+, K^+, Mg^{2+}, or Zn^{2+}, or no additional metal ions (black bars), and after the addition of 1 μM Ca^{2+} (red bars). Conditions: SiNW-Ss 0.95 mg/mL, PBS buffer (10 mM, pH = 7.3), λ_{ex} = 488 nm, RT.

SiNW-S displayed a favorable selectivity for Ca^{2+}. Additionally, the fluorescence response of the SiNW-S toward Ca^{2+} in the presence of these ions was also studied (red bar). Although the solution contained Mg^{2+}, Zn^{2+}, K^+, or Na^+ ions, the addition of Ca^{2+} noticeably altered the normalized I_{green}/I_{red}. We confirmed that the presence of common relevant metal ions does not remarkably alter the detection of Ca^{2+}.[32] In addition, SiNW-Ss were dispersed in PBS buffer solutions containing ionomycin (an ionophore to increase the intracellular Ca^{2+} concentration) and solution containing 10% BSA. The normalized I_{green}/I_{red} of the SiNW-Ss displayed little change (Figure S2), indicating that the ionomycin and protein had no influence on the emission of SiNW-Ss.

To actively position the SiNW-S in a single cell for the detection of Ca^{2+}, we loaded the SiNW-S at the tip of a micropipette via a micro-operation system. Figure 5 illustrates the loading scheme (Figure 5a) and shows the SEM image of the micropipette loaded with the SiNW-S (Figure 5b). Then, the SiNW-S loaded in the tip was inserted into the cell with the assistance of the Nikon A1 LSCM (illustrated in Figure 5c, and a video showing the insertion of the SiNW-S, video S1, is presented in the Supporting Information). Here, L929 cells were employed as a model to confirm that the sensors can be inserted in the cell, and even two sensors can be inserted in one cell for Ca^{2+} detection. L929 cells were stained with Hoechst33342 (a nuclear stain with a blue color) to facilitate observations under the LSCM. As shown in the Z-series fluorescence images (video S2), two fluorescence emissions were observed. The blue fluorescence was derived from the cell nucleus stained with Hoechst33342, and the red fluorescence was obtained from the SiNW-S. Figure S3 shows bright field images of the SiNW-S (in the red circle) before (Figure S3a) and after (Figure S3b) it was inserted into the L929 cell. Clearly, the SiNW-S is much smaller than the cell, which guaranteed little damage to the cell membrane during penetration with the SiNW-S. The safety of the insertion of the SiNW-S into the cells was further confirmed from the bright field video (video S3 in the Supporting Information).

Two SiNW-Ss, numbered S1 and S2, were utilized to detect the Ca^{2+} ions in different locations in an L929 cell. Initially, the fluorescence images of S1 and S2 were captured in 1 mL of PBS (Figure 6a). By observing the fluorescence images from the green and red channel of the LSCM, we found that the green fluorescence intensity of S1 and S2 was weak, and only the red fluorescence was detected (Figure 6e,i). However,

https://dx.doi.org/10.1021/acschemneuro.0c00041
ACS Chem. Neurosci. 2020, 11, 1283–1290

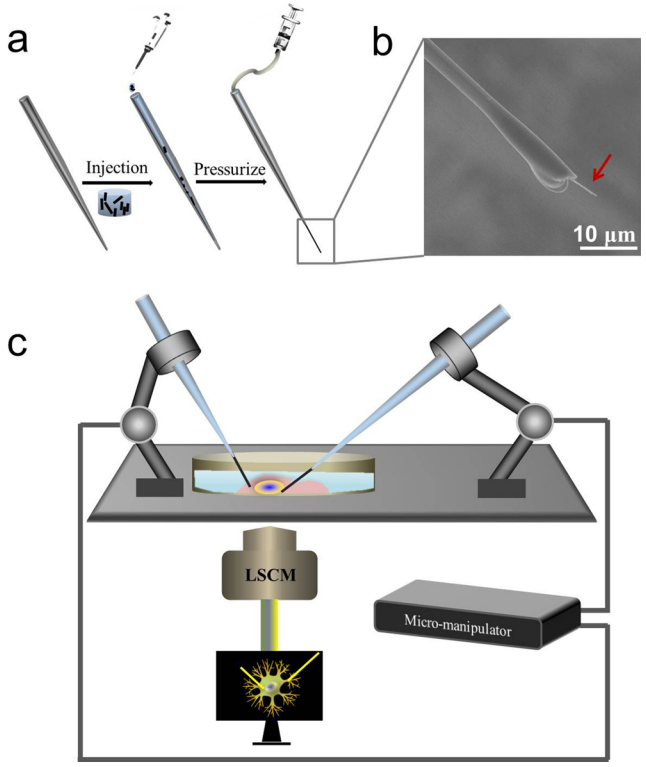

Figure 5. (a) Loading scheme of the SiNW-S with a micropipette. (b) SEM image of the SiNW-S at the tip of the micropipette. The red arrow points to a single SiNW-S. (c) Schematic of the detection system for the single nanowire-based ratiometric biosensor for Ca^{2+} in a single cell.

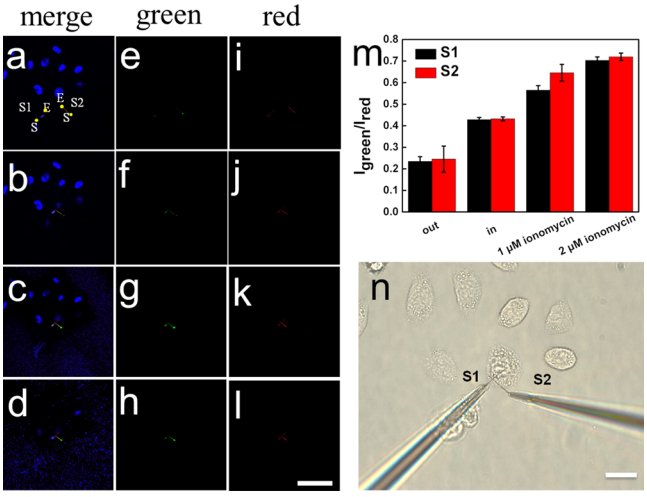

Figure 6. (a–l) Fluorescence images of S1, S2, and the L929 cell. (a) Images of S1 and S2 before insertion in the L929 cell. (b) Images of S1 and S2 inserted into the L929 cell. (c) Images captured after the addition of 1 μL of ionomycin; the concentration of the ionomycin in the extracellular media of the cells was 1 μM. (d) Images captured after the addition of another 1 μL of ionomycin; the concentration of the ionomycin in the extracellular media of the cells was 2 μM. (e–h) Images from green channel. (i–l) Images from red channel. (m) I_{green}/I_{red} of S1 and S2 in panels a–d. (n) Bright field images of S1 and S2 inserted into the cell. The scale bar represents 20 μm. Conditions: 10 mM PBS buffer, pH = 7.3, lasers with excitation wavelengths of 488 and 405 nm, RT. The error bars were generated by selecting three different locations of S1 and S2 and integrating their fluorescence intensities.

when S1 and S2 were inserted into the L929 cell (Figure 6b), the fluorescence intensity from the green channel increased, and the red fluorescence intensity exhibited little change (Figure 6f,j). The increase in the green fluorescence was attributed to the increase in the amount of Ca^{2+} in the cytoplasm, as evidenced by the emission from the molecule Fluo-3 on the surface the SiNW-S. The application of the ionophore ionomycin increases intracellular Ca^{2+}.[35] Therefore, various concentrations of ionomycin were added to the culture medium, and the fluorescence images of S1 and S2 were observed. As shown in Figure 6c, the green fluorescence was significantly increased after ionomycin was added into the culture medium (the concentration of the ionomycin in the medium was 1 μM) (Figure 6g). Further, little change in the red fluorescence intensity (Figure 6k) was observed. After more ionomycin was added to the medium (the concentration of the ionomycin in the medium was 2 μM, Figure 6d), the green fluorescence intensity was further increased (Figure 6h). However, a minimal change in the red fluorescence intensity was detected (Figure 6l). The increase in the green fluorescence was attributed to the Ca^{2+} outflow from organelles induced by ionomycin.[36] The change in the blue emission in the nucleus was due to the incubation with ionomycin, as a long incubation with ionomycin could decrease the cellular activity.[37−39] The green fluorescence intensities and red fluorescence intensities scanned along the direction from S to E of S1 and S2 in Figure 6a–d were recorded, and the I_{green}/I_{red} of S1 and S2 under different conditions are shown in Figure 6m. We selected three different sites in S1 and S2 and integrated their fluorescence intensities, and error bars were generated. As shown in Figure 6m, the I_{green}/I_{red} of S1 and S2 had almost no difference when they were out of the cell, but they were increased as the Ca^{2+} concentration increased in L929 cells. Moreover, the final values of I_{green}/I_{red} of S1 and S2 were almost the same, because the two sensors were close to each other. The bright field image indicated that the L929 cell survived even after S1 and S2 were inserted into the cell (Figure 6n). These data indicate that the sensors could be inserted into the cell at the same time and they has the capability to detect the Ca^{2+} in a living single cell simultaneously.

Ca^{2+} is vital in the body and neurites of a neuron. The regulation of the Ca^{2+} signal between the body and neurites is closely associated with some neurodegenerative diseases, such as Alzheimer's, Parkinson's, or Huntington's disease.[6,36,40] Here, the Ca^{2+} in the body and neurites of hippocampal neurons from fetal rats were detected with two SiNW-Ss, L1 and L2. First, fluorescence images were captured for both L1 and L2 in PBS (Figure 7a). By observing fluorescence from the green and red channels, we detected weak green fluorescence intensity for L1 and L2, and only red fluorescence was observed (Figure 7e,i). With the assistance of the micromanipulator, L1 was inserted into the body and L2 was inserted into the neurites. The green fluorescence intensity of L1 and L2 increased, and the red fluorescence intensity exhibited minimal changes (Figure 7b,f,j). The increase in the green emission was attributed to the presence of the Ca^{2+} in the cell. Subsequently, various concentrations of ionomycin were added to the culture medium. As shown in Figure 7c, the green fluorescence intensities of L1 and L2 were further increased (Figure 7g), while the red fluorescence intensities of L1 and L2 exhibited little change after the addition of ionomycin to the culture medium (the final concentration of

https://dx.doi.org/10.1021/acschemneuro.0c00041
ACS Chem. Neurosci. 2020, 11, 1283−1290

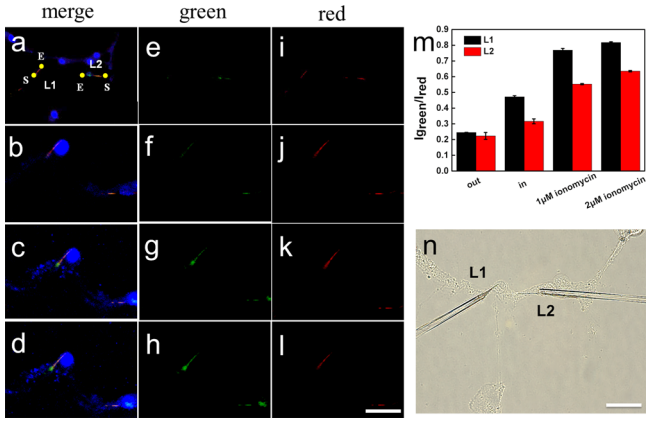

Figure 7. (a–l) Fluorescence images of L1, L2, and a hippocampal neuron from a fetal rat. (a) Image of L1 and L2 in PBS. (b) Image of L1 and L2 inserted into a hippocampal neuron. (c) Image of L1 and L2 in the hippocampal neuron after the addition of ionomycin to the culture medium (the concentration of the ionomycin in the medium of the cells was 1 μM). (d) Image captured after the subsequent addition of more ionomycin (the concentration of the ionomycin in the medium of the cells was 2 μM). (e–h) Images from the green channel. (i–l) Images from the red channel. (m) Change in the I_{green}/I_{red} values of L1 and L2 under various conditions. (n) Bright field image of L1 and L2 after insertion into a hippocampal neuron. The scale bar represents 20 μm. Conditions: 1 mL of 10 mM PBS buffer, pH = 7.3; lasers with excitation wavelengths of 488 and 405 nm, RT. The error bars were generated by selecting three different sites of L1 and L2 and integrating their fluorescence intensities.

the ionomycin in the medium was 1 μM) and stabilization for 2 min (Figure 7k). Furthermore, the addition of more ionomycin (the final concentration of the ionomycin in the medium was 2 μM) to the culture medium (Figure 7d) resulted in a further increase in the green fluorescence intensities (Figure 7h) but did not alter the red fluorescence intensities (Figure 7l). The intensities of the green fluorescence and red fluorescence from L1 and L2 were scanned along the direction from S to E and recorded, as shown in Figure 7a–d, and the I_{green}/I_{red} values of L1 and L2 under different experimental conditions were obtained. The data were recorded three times at various locations of L1 and L2, and error bars were generated. The I_{green}/I_{red} values of L1 and L2 for four conditions are shown in Figure 7m. The I_{green}/I_{red} values were low when L1 and L2 were only incubated in PBS. After L1 and L2 were inserted into the cell and ionomycin was subsequently added into cell culture medium, the I_{green}/I_{red} obviously increased. Moreover, the I_{green}/I_{red} differed for L1 and L2 at every step. The change in I_{green}/I_{red} was more significant in the cell body than in the neurites, in contrast to the observations from the L929 cell. Based on this evidence, the content of Ca^{2+} ions in the neuronal body was higher than that in the neurites.[41] We also captured bright field images of L1, L2, and the cell (Figure 7n). The bright field images revealed that the rat hippocampal neuron was still alive after L1 and L2 were inserted into the cell, confirming the safety of the sensor in neurons.

CONCLUSIONS

In summary, a SiNW-based ratiometric fluorescence sensor for Ca^{2+} was constructed by introducing the ruthenium-based dye with red emission as the reference molecule and Fluo-3 with green emission as the response molecule on the surface of SiNWs. The sensors displayed a favorable selectivity and anti-interference ability from other metal ions, and they achieved a reversible detection of Ca^{2+} in PBS. In particular, with the help of a micromanipulator, SiNW-S was loaded in the tip of a micropipette and was able to recognize the difference between the concentrations of Ca^{2+} ions in the cell body and the neurites of a neuron. The SiNW-S profiled the heterogeneity of the Ca^{2+} in an individual cell with a high spatial resolution. This sensor provides a new intriguing method for detection in single cells and even for monitoring dynamic changes.

METHODS

Materials and Equipment. Fluo-3 was purchased from Dojindo Laboratories in Japan. 3-Aminopropyltriethoxysilane (APTES) and ionomycin were purchased from J&K Scientific Ltd. HF (40%) was purchased from Aladdin. Hoechst33342, $Ru(bpy)_2$(mcbpy-O-Su-ester)$(PF_6)_2$, 1-(3-dimethylaminopropyl)-3-ethylcarbodiimide hydrochloride (EDC), and *N*-hydroxysuccinimide (NHS) were purchased from Sigma-Aldrich. Other reagents were purchased from Beijing Chemical Regent Co. The chemicals and reagents used in this study were AR grade.

SEM images were captured by using a Hitachi S-4800FEG scanning electron microscope. TEM images were captured by using a JEOL-2100F transmission electron microscope (acceleration voltage = 200 kV). The X-ray photoelectron spectroscopy (XPS) spectra were recorded with a Thermo Fisher Scientific ESCALAB 250Xi X-ray photoelectron spectroscope (voltage = 15 kV). The MP-285 micromanipulator was employed to insert the single SiNW sensors into a single cell. Fluorescence images of the cells and single SiNW sensors were captured with a Nikon A1 LSCM equipped with a 60× oil-immersion objective lens at excitation wavelengths of 488 nm from the green and red channel.

Preparation of SiNW-based Sensors. SiNWs arrays with different lengths were fabricated by chemical etching (CE) and heated to 400 °C in a furnace for 200 min to obtain a silica shell. The SiNWs-a was immersed in a solution of H_2SO_4 (98%) and 30% H_2O_2 (3:1, v/v) at 95 °C for 1 h and repeatedly washed with deionized water. Then, the SiNW-a was immersed in a solution of H_2O, 30% H_2O_2, and NH_4OH (5:1:1, v/v/v) for 1.5 h at room temperature, repeatedly rinsed with deionized , and dried under vacuum. The product was SiNWs-a-OH. The dried SiNWs-a-OH was immersed in 15 mL of anhydrous toluene (distilled) in a round-bottomed flask under a nitrogen flow. Then, 100 μL of APTES was added. The solution was heated to 90 °C for another 24 h under a nitrogen atmosphere. The wafers were picked out and washed repeatedly with ethanol. The wafer was SiNWs-a-NH_2. SiNWs-a-NH_2 was immersed in 2 mL of PBS solution (10 mM, pH = 7.3), and 200 μL of $Ru(bpy)_2$(mcbpy-O-Su-ester)$(PF_6)_2$ solution (5 mg/mL, in DMF) was added to the PBS solution for 5 h at room temperature. The wafer was picked out and washed with deionized water. The wafer was SiNWs-a-Ru. Next, 1 mL of Fluo-3 (1 mg/mL, in DMSO), 800 μL of EDC (0.1 mg/mL, in ultrapure water), and 500 μL of NHS (0.1 mg/mL, in ultrapure water) were sequentially added to 2 mL of ultrapure water at 0 °C and stirred for 30 min to activate the carboxyl in Fluo-3. Finally, the SiNWs-a-Ru was added into the 2 mL solution described above and oscillated for another 5 h. The wafer was picked out and washed repeatedly with ultrapure water. To confirm that the unreacted molecules were completely removed from the product, we monitored the fluorescence of the wash liquid until fluorescence was not detected. The modified SiNWs array with the two molecules on a Si wafer were SiNWs-A. The SiNWs-A with short SiNWs was used to detect Ca^{2+} in solution. The SiNWs-A with long SiNWs was ultrasonicated in ultrapure water, to drop off the SiNWs from Si wafer to obtain the stock solution of the single SiNW sensors (final concentration 0.95 mg/mL). The single SiNW sensor was designated as SiNW-S, which was employed to detect Ca^{2+} in a single cell.

Loading of the SiNW-S into the Nanopipettes. First, micropipettes with a tip diameter of 0.5–0.9 μm were fabricated

https://dx.doi.org/10.1021/acschemneuro.0c00041
ACS Chem. Neurosci. 2020, 11, 1283–1290

from a thin-walled borosilicate capillary (Sutter, BF100-78-10, melting point 498 °C) with a micropipette puller (Sutter P-97). Next, 5 μL of a diluted stock solution of the SiNW-S was injected into the micropipette by a pipettor with a 10 μL pipet tip and subsequently pushed with a syringe until a SiNW-S with the proper length was exposed at the tip of the micropipette. This process was performed with the assistance of a micromanipulator and microscope. Finally, the micropipettes loaded with SiNW-S were dried in air at ambient temperature for the subsequent detection of intracellular Ca^{2+}.

Cell Culture. L929 cells were purchased from the Center of Cells, Peking Union Medical College. Before capturing fluorescence images, L929 cells were cultured in confocal microscope dishes containing DMEM. The dishes were maintained in a 5% CO_2 air atmosphere at 37 °C in a humidified Panasonic MCO-5AC incubator. Primary rat hippocampal neurons were extracted from the hippocampus of Wistar rat embryos (E17−E18). First, the hippocampus was cut into small pieces and treated with trypsin (0.25%) for 15 min (37 °C) in Ca^{2+}- and Mg^{2+}-free Hank's balanced salt solution (HBSS). Then, the activity of the residual trypsin was quenched by adding DMEM containing 10% BSA. The small pieces of the hippocampus were transferred to a neurobasal medium supplemented with B27 (1:50 dilution) and GlutaMAXTM-1 (1:100). The neurons were dissociated in neurobasal medium and then seeded onto the glass bottoms of the 35 mm dishes that have been coated with poly(D-lysine) (0.1 mg/mL) at a density of (4.0−5.0) × 10^5 cells/dish. The dishes with the neurons were maintained in a humidified incubator with 5% CO_2 at 37 °C. The hippocampal neurons were cultured for 7 days before the cell experiments. All experimental protocols were approved by the Institutional Animal Care and Use Committee (IACUC number 2018-039, National Beijing Center for Drug Safety Evaluation and Research, Beijing, China).

■ ASSOCIATED CONTENT

Supporting Information

The Supporting Information is available free of charge at https://pubs.acs.org/doi/10.1021/acschemneuro.0c00041.

Experimental methods for the preparation of SiNWs, fluorescence detection of the SiNW-S, XPS spectrum of SiNWs, bright field images of the SiNW-S out and in the L929 cell (PDF)

Procedure for the insertion of the SiNW-S to an L929 cell (AVI)

Z-scan fluorescence images of the L929 cell and the 4 SiNW-S inserted into the cell (AVI)

Procedure for removing the SiNW-S from the L929 cells (AVI)

■ AUTHOR INFORMATION

Corresponding Author

Lixuan Mu − *Key Laboratory of Photochemical Conversion and Optoelectronic Materials, Technical Institute of Physics and Chemistry, Chinese Academy of Sciences, Beijing 100190, China;* orcid.org/0000-0002-6613-5368; Phone: 86-10-82543513; Email: mulixuan@mail.ipc.ac.cn

Authors

Min Chen − *Key Laboratory of Photochemical Conversion and Optoelectronic Materials, Technical Institute of Physics and Chemistry, Chinese Academy of Sciences, Beijing 100190, China; University of Chinese Academy of Sciences, Beijing 100049, China*

Shuai Wang − *State Key Laboratory of Toxicology and Medical Countermeasures, Institutes of Pharmacology and Toxicology, Academy of Military Medical Sciences, Beijing 100850, China*

Xingxing Cao − *Key Laboratory of Photochemical Conversion and Optoelectronic Materials, Technical Institute of Physics and Chemistry, Chinese Academy of Sciences, Beijing 100190, China; University of Chinese Academy of Sciences, Beijing 100049, China*

Sen Liang − *Key Laboratory of Photochemical Conversion and Optoelectronic Materials, Technical Institute of Physics and Chemistry, Chinese Academy of Sciences, Beijing 100190, China; University of Chinese Academy of Sciences, Beijing 100049, China*

Yuan Wang − *Key Laboratory of Photochemical Conversion and Optoelectronic Materials, Technical Institute of Physics and Chemistry, Chinese Academy of Sciences, Beijing 100190, China; University of Chinese Academy of Sciences, Beijing 100049, China*

Guangwei She − *Key Laboratory of Photochemical Conversion and Optoelectronic Materials, Technical Institute of Physics and Chemistry, Chinese Academy of Sciences, Beijing 100190, China;* orcid.org/0000-0003-1017-5456

Jun Yang − *State Key Laboratory of Toxicology and Medical Countermeasures, Institutes of Pharmacology and Toxicology, Academy of Military Medical Sciences, Beijing 100850, China;* orcid.org/0000-0002-4901-8530

Yongan Wang − *State Key Laboratory of Toxicology and Medical Countermeasures, Institutes of Pharmacology and Toxicology, Academy of Military Medical Sciences, Beijing 100850, China*

Wensheng Shi − *Key Laboratory of Photochemical Conversion and Optoelectronic Materials, Technical Institute of Physics and Chemistry, Chinese Academy of Sciences, Beijing 100190, China; University of Chinese Academy of Sciences, Beijing 100049, China;* orcid.org/0000-0001-5747-4862

Complete contact information is available at: https://pubs.acs.org/10.1021/acschemneuro.0c00041

Author Contributions

L.M. and W.S. designed the experiments; M.C. performed the research with the aid of X.C.; S.W., J.Y., and Y.a.W. provided help for M.C. to isolate the rat hippocampal neurons; S.L., Y.W., and G.S. contributed to data analysis; M.C. and L.M. wrote the manuscript with the help from W.S. All the authors read and approved the final manuscript.

Notes

The authors declare no competing financial interest.

■ ACKNOWLEDGMENTS

This work was supported by National Key R&D Program of China (2017YFE0196400; 2016YFA0200800), NSFC (51672284, 21975269), Beijing Natural Science Foundation (2181002), and Chinese Academy of Sciences (1A1111KYSB20180017, QYZDJ-SSW-JSC032, XDB17000000).

■ REFERENCES

(1) Grienberger, C., and Konnerth, A. (2012) Imaging calcium in neurons. *Neuron* 73 (5), 862−85.

(2) Rossol, M., Pierer, M., Raulien, N., Quandt, D., Meusch, U., Rothe, K., Schubert, K., Schoneberg, T., Schaefer, M., Krugel, U., Smajilovic, S., Brauner-Osborne, H., Baerwald, C., and Wagner, U. (2012) Extracellular Ca^{2+} is a danger signal activating the NLRP3 inflammasome through G protein-coupled calcium sensing receptors. *Nat. Commun.* 3, 1329.

(3) Alonso, M. T., Rojo-Ruiz, J., Navas-Navarro, P., Rodriguez-Prados, M., and Garcia-Sancho, J. (2017) Measuring Ca(2+) inside intracellular organelles with luminescent and fluorescent aequorin-

based sensors. *Biochim. Biophys. Acta, Mol. Cell Res. 1864* (6), 894−899.
(4) Stringer, C., and Pachitariu, M. (2019) Computational processing of neural recordings from calcium imaging data. *Curr. Opin. Neurobiol. 55*, 22−31.
(5) Chiacchiaretta, M., Bramini, M., Rocchi, A., Armirotti, A., Giordano, E., Vazquez, E., Bandiera, T., Ferroni, S., Cesca, F., and Benfenati, F. (2018) Graphene oxide upregulates the homeostatic functions of primary astrocytes and modulates astrocyte-to-neuron communication. *Nano Lett. 18* (9), 5827−5838.
(6) Heredia, D. J., Feng, C. Y., Agarwal, A., Nennecker, K., Hennig, G. W., and Gould, T. W. (2018) Postnatal restriction of activity-induced Ca(2+) responses to schwann cells at the neuromuscular junction are caused by the proximo-distal loss of axonal synaptic vesicles during development. *J. Neurosci. 38* (40), 8650−8665.
(7) Si, D., Epstein, T., Koo Lee, Y.-E., and Kopelman, R. (2012) Nanoparticle PEBBLE sensors for quantitative nanomolar imaging of intracellular free calcium ions. *Anal. Chem. 84* (2), 978−86.
(8) Martin, V., Vale, C., Hirama, M., Yamashita, S., Rubiolo, J. A., Vieytes, M. R., and Botana, L. M. (2015) Synthetic ciguatoxin CTX 3C induces a rapid imbalance in neuronal excitability. *Chem. Res. Toxicol. 28* (6), 1095−108.
(9) Berridge, M. J. (1993) Inositol trisphosphate and calcium signalling. *Nature 361* (6410), 315−325.
(10) O'Neill, B. K., and Laughlin, S. T. (2018) Neuronal calcium recording with an engineered TEV protease. *ACS Chem. Biol. 13* (5), 1159−1164.
(11) Sui, B., Liu, X., Wang, M., and Belfield, K. D. (2016) A highly selective fluorescence turn-on sensor for extracellular calcium ion detection. *Chem. - Eur. J. 22* (30), 10351−4.
(12) Sulmann, S., Wallisch, M., Scholten, A., Christoffers, J., and Koch, K. W. (2016) Mapping calcium-sensitive regions in the neuronal calcium sensor GCAP2 by site-specific fluorescence labeling. *Biochemistry 55* (18), 2567−77.
(13) Roberts, S., Seeger, M., Jiang, Y., Mishra, A., Sigmund, F., Stelzl, A., Lauri, A., Symvoulidis, P., Rolbieski, H., Preller, M., Dean-Ben, X. L., Razansky, D., Orschmann, T., Desbordes, S. C., Vetschera, P., Bach, T., Ntziachristos, V., and Westmeyer, G. G. (2018) Calcium sensor for photoacoustic imaging. *J. Am. Chem. Soc. 140* (8), 2718−2721.
(14) Wang, S. Q., Zhao, H., Wang, Y., Li, C. M., Chen, Z. H., and Paulose, V. (2008) Silver-coated near field optical scanning microscope probes fabricated by silver mirror reaction. *Appl. Phys. B: Lasers Opt. 92* (1), 49−52.
(15) Ponsot, F., Shen, W., Ashokkumar, P., Audinat, E., Klymchenko, A. S., and Collot, M. (2017) PEGylated red-emitting calcium probe with improved sensing properties for neuroscience. *ACS Sens 2* (11), 1706−1712.
(16) Badura, A., Sun, X. R., Giovannucci, A., Lynch, L. A., and Wang, S. S. (2014) Fast calcium sensor proteins for monitoring neural activity. *Neurophotonics 1* (2), 025008.
(17) Nevian, T., and Helmchen, F. (2007) Calcium indicator loading of neurons using single-cell electroporation. *Pfluegers Arch. 454* (4), 675−688.
(18) Yan, F., Bai, Z., Ma, T., Sun, X., Zu, F., Luo, Y., and Chen, L. (2019) Surface modification of carbon quantum dots by fluorescein derivative for dual-emission ratiometric fluorescent hypochlorite biosensing and in vivo bioimaging. *Sens. Actuators, B 296*, 126638.
(19) Takahashi, A., Camacho, P., Lechleiter, J. D., and Herman, B. (1999) Measurement of intracellular calcium. *Physiol. Rev. 79*, 1089−1125.
(20) Paredes, R. M., Etzler, J. C., Watts, L. T., Zheng, W., and Lechleiter, J. D. (2008) Chemical calcium indicators. *Methods 46* (3), 143−51.
(21) Cao, D., Liu, Z., Verwilst, P., Koo, S., Jangjili, P., Kim, J. S., and Lin, W. (2019) Coumarin-based small-molecule fluorescent chemosensors. *Chem. Rev. 119*, 10403−10519.
(22) Carter, K. P., Young, A. M., and Palmer, A. E. (2014) Fluorescent sensors for measuring metal ions in living systems. *Chem. Rev. 114*, 4564−4601.
(23) Son, D., Park, S. Y., Kim, B., Koh, J. T., Kim, T. H., An, S., Jang, D., Kim, G. T., Jhe, W., and Hong, S. (2011) Nanoneedle Transistor-Based Sensors for the Selective Detection of Intracellular Calcium Ions. *ACS Nano 5* (5), 3888−3895.
(24) Gao, Y., Longenbach, T., Vitol, E. A., Orynbayeva, Z., Friedman, G., and Gogotsi, Y. (2014) One-dimensional nanoprobes for single-cell studies. *Nanomedicine 9* (1), 153−168.
(25) Robinson, J. T., Jorgolli, M., Shalek, A. K., Yoon, M. H., Gertner, R. S., and Park, H. (2012) Vertical nanowire electrode arrays as a scalable platform for intracellular interfacing to neuronal circuits. *Nat. Nanotechnol. 7* (3), 180−4.
(26) Cui, Y., Wei, Q., Park, H., and Lieber, C. M. (2001) Nanowire nanosensors for highly sensitive and selective detection of biological and chemical species. *Science 293* (5533), 1289.
(27) Chiappini, C., Campagnolo, P., Almeida, C. S., Abbassi-Ghadi, N., Chow, L. W., Hanna, G. B., and Stevens, M. M. (2015) Mapping local cytosolic enzymatic activity in human esophageal mucosa with porous silicon nanoneedles. *Adv. Mater. 27*, 5147−5152.
(28) Chiappini, C., De Rosa, E., Martinez, J. O., Liu, X., Steele, J., Stevens, M. M., and Tasciotti, E. (2015) Biodegradable silicon nanoneedles delivering nucleic acids intracellularly induce localized in vivo neovascularization. *Nat. Mater. 14*, 532−539.
(29) Fromherz, P., and Voelker, M. (2009) Comment on "Detection, stimulation, and inhibition of neuronal signals with high-density nanowire transistor arrays&quot. *Science 323* (5920), 1429b.
(30) Kim, W., Ng, J. K., Kunitake, M. E., Conklin, B. R., and Yang, P. (2007) Interfacing silicon nanowires with mammalian cells. *J. Am. Chem. Soc. 129* (23), 7228−7229.
(31) Cao, X., Mu, L., Chen, M., Bu, C., Liang, S., She, G., and Shi, W. (2018) Single silicon nanowire-based fluorescent sensor for endogenous hypochlorite in an individual cell. *Adv. Biosys. 2*, 1800213.
(32) Minta, A., Kao, J. P. Y., and Tsien, R. Y. (1989) Fluorescence indicators for cytosolic calcium based on rhodamine and fluorescein chromophores. *J. Biol. Chem. 264*, 8171−8178.
(33) Gaillard, S., Yakovlev, A., Luccardini, C., Oheim, M., Feltz, A., and Mallet, J.-M. (2007) Synthesis and characterization of a new red-emitting Ca^{2+} indicator, calcium ruby. *Org. Lett. 9*, 2629−2632.
(34) Sixt, T., Sieger, M., Krafft, M. J., Bubrin, D., Fiedler, J., and Kaim, W. (2010) Ambi-valence taken literally: ruthenium vs iron oxidation in (1,1′-diphosphinoferrocene)ruthenium(II) hydride and chloride complexes as deduced from spectroelectrochemistry of the heterodimetallic "mixed-valent" intermediates. *Organometallics 29* (21), 5511−5516.
(35) Toeplitz, B. K., Cohen, A. I., Funke, P. T., Parker, W. L., and Gougoutas, J. Z. (1979) Structure of ionomycin - a novel diacidic polyether antibiotic having high affinity for calcium ions. *J. Am. Chem. Soc. 101* (12), 3344−3353.
(36) Wojda, U., Salinska, E., and Kuznicki, J. (2008) Calcium ions in neuronal degeneration. *IUBMB Life 60* (9), 575−90.
(37) Johnson, J. R., Kocher, B., Barnett, E. M., Marasa, J., and Piwnica-Worms, D. (2012) Caspase-activated cell-penetrating peptides reveal temporal coupling between endosomal release and apoptosis in an RGC-5 cell model. *Bioconjugate Chem. 23* (9), 1783−1793.
(38) Takei, Y., Arai, S., Murata, A., Takabayashi, M., Oyama, K., Ishiwata, S. i., Takeoka, S., and Suzuki, M. (2014) A Nanoparticle-based ratiometric and self-calibrated fluorescent thermometer for single living cells. *ACS Nano 8* (1), 198−206.
(39) Zou, H., Limpert, A. S., Zou, J., Dembo, A., Lee, P. S., Grant, D., Ardecky, R., Pinkerton, A. B., Magnuson, G. K., Goldman, M. E., Rong, J., Teriete, P., Sheffler, D. J., Reed, J. C., and Cosford, N. D. (2015) Benzodiazepinone derivatives protect against endoplasmic reticulum stress-mediated cell death in human neuronal cell lines. *ACS Chem. Neurosci. 6* (3), 464−75.

https://dx.doi.org/10.1021/acschemneuro.0c00041
ACS Chem. Neurosci. 2020, 11, 1283−1290

(40) Xu, M., Pan, R., Zhu, Y., Jiang, D., and Chen, H. Y. (2019) Molecular profiling of single axons and dendrites in living neurons using electrosyringe-assisted electrospray mass spectrometry. *Analyst 144* (3), 954−960.
(41) Liu, Z., Jing, X., Zhang, S., and Tian, Y. (2019) A Copper Nanocluster-Based Fluorescent probe for real-time imaging and ratiometric biosensing of calcium ions in neurons. *Anal. Chem. 91* (3), 2488−2497.

https://dx.doi.org/10.1021/acschemneuro.0c00041
ACS Chem. Neurosci. 2020, 11, 1283−1290